Cosmological parameter determination in free-form strong gravitational lens modelling

Lubini, M ; Sereno, M ; Coles, J ; Jetzer, P ; Saha, P

Abstract: We develop a novel statistical strong-lensing approach to probe the cosmological parameters by exploiting multiple redshift image systems behind galaxies or galaxy clusters. The method relies on free-form mass inversion of strong lenses and does not need any additional information other than gravitational lensing. Since in free-form lensing the solution space is a high-dimensional convex polytope, we consider Bayesian model comparison analysis to infer the cosmological parameters. The volume of the solution space is taken as a tracer of the probability of the underlying cosmological assumption. In contrast to parametric mass inversions, our method accounts for the mass-sheet degeneracy, which implies a degeneracy between the steepness of the profile and the cosmological parameters. Parametric models typically break this degeneracy, introducing hidden priors to the analysis that contaminate the inference of the parameters. We test our method with synthetic lenses, showing that it is able to infer the assumed cosmological parameters. Applied to the Cluster Lensing And Supernova survey with Hubble (CLASH) clusters, the method might be competitive with other probes.

DOI: https://doi.org/10.1093/mnras/stt2057

Monthly Notices
of the
ROYAL ASTRONOMICAL SOCIETY

MNRAS **437,** 2461–2470 (2014)
Advance Access publication 2013 November 30

doi:10.1093/mnras/stt2057

Cosmological parameter determination in free-form strong gravitational lens modelling

M. Lubini,[1]⋆ M. Sereno,[2,3] J. Coles,[1] Ph. Jetzer[1] and P. Saha[1]

[1] *Institut für Theoretische Physik, Universität Zürich, Winterthurerstrasse 190, CH-8057 Zürich, Switzerland*
[2] *Dipartimento di Scienza Applicata e Tecnologia, Politecnico di Torino, Corso Duca degli Abruzzi 24, I-10129 Torino, Italia*
[3] *INFN, Sezione di Torino, Via Pietro Giuria 1, I-10125 Torino, Italia*

Accepted 2013 October 23. Received 2013 September 24; in original form 2013 April 26

ABSTRACT

We develop a novel statistical strong-lensing approach to probe the cosmological parameters by exploiting multiple redshift image systems behind galaxies or galaxy clusters. The method relies on free-form mass inversion of strong lenses and does not need any additional information other than gravitational lensing. Since in free-form lensing the solution space is a high-dimensional convex polytope, we consider Bayesian model comparison analysis to infer the cosmological parameters. The volume of the solution space is taken as a tracer of the probability of the underlying cosmological assumption. In contrast to parametric mass inversions, our method accounts for the mass-sheet degeneracy, which implies a degeneracy between the steepness of the profile and the cosmological parameters. Parametric models typically break this degeneracy, introducing hidden priors to the analysis that contaminate the inference of the parameters. We test our method with synthetic lenses, showing that it is able to infer the assumed cosmological parameters. Applied to the Cluster Lensing And Supernova survey with Hubble (CLASH) clusters, the method might be competitive with other probes.

Key words: gravitational lensing: strong – methods: statistical – cosmological parameters.

1 INTRODUCTION

Estimates of the matter/energy content of the Universe have reached uncertainties of only a few per cent through the combined analysis of the anisotropy measurements of the cosmic microwave background (CMB; Komatsu et al. 2011; Planck Collaboration et al. 2013), the observation of the baryon acoustic oscillations (BAOs) in the distribution of galaxies (Percival et al. 2010) and the luminosity distance of Type Ia supernovae (Amanullah et al. 2010; Riess et al. 2011). Nonetheless, the precision cosmology era crucially requires further independent methods in order to control systematic effects that can plague some techniques and to break statistical degeneracies.

A unique tool is provided by gravitational lensing, which can furnish a rich source of information about the underlying cosmological model. Gravitational lensing relies on the angular diameter distances, which in turn depend on the matter/energy content of the Universe. Particularly in galaxy clusters, the identification of multiple gravitationally lensed background sources located at different redshifts (e.g. Limousin et al. 2007; Richard et al. 2009) supplies information on the cosmological parameters. Galaxies as lenses can probe the cosmology too, but only a few multiple source redshift lenses are presently known (Bolton et al. 2008).

Unlike other probes, such as supernova measurements, the cosmological information contained in strong gravitational lenses is purely geometrical and does not require any kind of calibration. Moreover, it probes cosmology in an almost unexplored redshift range of around $z \sim 3$–4. Various other works (e.g. Golse, Kneib & Soucail 2002; Sereno 2002; Sereno & Longo 2004; Soucail, Kneib & Golse 2004; Gilmore & Natarajan 2009; D'Aloisio & Natarajan 2011; Zieser & Bartelmann 2012) have shown and investigated the ability of strong gravitational lensing to determine the cosmological parameters in clusters of galaxies using parametric lensing models. Jullo et al. (2010) constrained the mass distribution of the main components of the galaxy cluster Abell 1689 and the dark energy equation of state.

Parametric models assume a functional form for the lens mass distribution and can be very efficient if all the cluster components are considered through adequate mass profiles. These models, however, introduce hidden priors to the analysis, as the assumed shape may unintentionally break possible degeneracies between the cosmological parameters and the mass profile. For instance, the NFW (Navarro, Frenk & White 1996, 1997) or isothermal density mass profiles can both provide good fits to observed systems, but choosing one of the two competitive profiles artificially breaks the mass-sheet degeneracy and biases the analysis of cosmological parameters.

The mass-sheet degeneracy is one of the main limitations and a source of uncertainty in gravitational lensing mass estimation (Falco, Gorenstein & Shapiro 1985; Saha 2000). A significant endeavour to break this degeneracy in parametric models has been made when modelling the mass profile of galaxies and

⋆ E-mail: lubini@physik.uzh.ch

galaxy clusters (e.g. Suyu et al. 2012; Collett et al. 2013; Greene et al. 2013; Umetsu 2013). Proper analyses of the mass-sheet degeneracy should then be considered when investigating the cosmological parameters.

Parametric models also demand deep knowledge of all the cluster components, which can only be achieved though observations other than gravitational lensing, e.g. optical for the position of the galactic haloes, and X-ray for the temperature and location of the intracluster medium (Voit 2005; Sereno, Lubini & Jetzer 2010; Limousin et al. 2013; Sereno et al. 2013). Only lensing clusters with deep multi-wavelength data sets can then be used to constrain cosmological parameters through parametric models.

In this paper, we apply a free-form approach to model the lens mass distribution. This approach only requires the knowledge of the lensed image positions and redshifts, and is more flexible than analytic models. Several different forms of the basic strategy have been developed for clusters with given cosmological parameters (Abdelsalam, Saha & Williams 1998a,b; Bradač, Lombardi & Schneider 2004; Bradač et al. 2005; Diego et al. 2005; Liesenborgs et al. 2007; Read, Saha & Macciò 2007; Coe et al. 2008; Deb, Goldberg & Ramdass 2008). In a given cosmology, the presence of sources at different redshifts helps break lensing degeneracies. In the present work, however, we do not fix the cosmology. Instead, we exploit the multiple source redshifts to follow a formulation of Occam's razor for the purpose of comparing competitive cosmological models. We consider a Bayesian approach exploiting the statistical dispersion of the parameter space describing the mass distribution to obtain information about the assumed cosmological model.

The layout of this paper is as follows. In Section 2, the cosmological information contained in strong gravitational lensing, as well as the relevant degeneracies, is stated, whereas the free-form lensing approach is laid out in Section 3. Section 4 presents the statistical method, which is based on Occam's razor in Bayesian model comparison, whereas in Section 5 we test the method through synthetic lenses and show that we are able to account for the mass-sheet degeneracy. The performance of the method in a realistic situation is shown in Section 6. Conclusions are presented in Section 7.

2 FRAMEWORK

The basic relation in gravitational lensing is the lens equation (Schneider, Ehlers & Falco 1992; Schneider, Kochanek & Wambsganss 2006)

$$\boldsymbol{\beta} = \boldsymbol{\theta} - \boldsymbol{\alpha}(\boldsymbol{\theta}), \tag{1}$$

which maps the observed image angular position $\boldsymbol{\theta}$ to the angular position $\boldsymbol{\beta}$ of the source through the scaled deflection angle

$$\boldsymbol{\alpha}(\boldsymbol{\theta}) = \frac{1}{\pi}\int_{\mathbb{R}^2} \kappa(\boldsymbol{\theta}')\frac{\boldsymbol{\theta}-\boldsymbol{\theta}'}{\left|\boldsymbol{\theta}-\boldsymbol{\theta}'\right|^2}\,\mathrm{d}\boldsymbol{\theta}'. \tag{2}$$

The dimensionless surface mass density or convergence κ is defined by

$$\kappa(\boldsymbol{\theta}) = \frac{\Sigma(D_{\mathrm{ol}}\boldsymbol{\theta})}{\Sigma_{\mathrm{crit}}} \quad \text{with} \quad \Sigma_{\mathrm{crit}} = \frac{c^2}{4\pi G}\frac{D_{\mathrm{os}}}{D_{\mathrm{ls}}D_{\mathrm{ol}}}, \tag{3}$$

where Σ is the surface mass density of the lens, and D_{ol}, D_{os} and D_{ls} are the angular diameter distances between the observer and lens, the observer and source, and the lens and source, respectively.

We consider a model of universe with cold dark matter (CDM) whose accelerated expansion is propelled by some form of dark energy. Assuming a dark energy with a constant equation of state w, the angular diameter distance between the redshifts z_{a} and z_{b} is (Weinberg 1972)

$$D_{\mathrm{ab}} = \frac{c}{(1+z_{\mathrm{b}})H_0\sqrt{|\Omega_k|}}\,\mathcal{S}_k\left(\sqrt{|\Omega_k|}\int_{z_{\mathrm{a}}}^{z_{\mathrm{b}}}\frac{H_0}{H(z)}\mathrm{d}z\right), \tag{4}$$

where $\mathcal{S}_k(x) = x$, $\sin(x)$ or $\sinh(x)$ for a flat, closed or open universe, respectively. The Hubble parameter $H(z)$ is given by

$$\frac{H(z)}{H_0} = \sqrt{\Omega_{\mathrm{m}}(1+z)^3 + \Omega_k(1+z)^2 + \Omega_{\mathrm{de}}(1+z)^{3(1+w)}}, \tag{5}$$

where $H_0 = 100\,h\,\mathrm{km\,s^{-1}\,Mpc^{-1}}$ is the Hubble constant with the dimensionless Hubble parameter h and the Ω are the matter, curvature k and dark energy density parameters. The standard ΛCDM model with cosmological constant Λ is given by the special case with $w = -1$ and $\Omega_{\mathrm{de}} = \Omega_\Lambda$.

2.1 Strong-lensing cosmography

The aim of this paper is to infer the cosmological parameters, which hereafter are simply denoted by Ω, through the distances in equation (3), exploiting strong-lensing observations in clusters of galaxies. Since what we observe are the angular positions $\boldsymbol{\theta}$ of the lensed images, by means of equation (1), gravitational lensing only deduces κ rather than the true mass profile Σ or any of the distances. However, when considering a lensing object where multiple sources are observed, κ can simultaneously be inferred at different source redshifts. As we are dealing with multiple source planes, whereas the observer and lens redshifts are fixed, κ depends only on the source redshift z_{s}. The source-dependent part

$$\Delta_{\mathrm{s}} = \frac{D_{\mathrm{ls}}}{D_{\mathrm{os}}} \tag{6}$$

can then be extracted from the convergence, which we rewrite as

$$\kappa(z_{\mathrm{s}}) = \Delta_{\mathrm{s}}\,\tilde{\kappa} = \Delta_{\mathrm{s}}\frac{\kappa_{\mathrm{ref}}}{\Delta_{\mathrm{ref}}}. \tag{7}$$

$\tilde{\kappa}$ can be interpreted as the convergence for a source geometrically at infinity, i.e. where $\Delta_{\mathrm{s}} = 1$, or alternatively one could consider the convergence κ_{ref} at some fixed reference source redshift z_{ref}.

In the case of a single source plane, $\tilde{\kappa}$ is completely degenerate with the distance ratio Δ_{s}, since gravitational lensing is only able to infer κ, and both $\tilde{\kappa}$ and Δ_{s} in equation (7) are unknown. Consequently, we cannot constrain the cosmological parameters Ω contained in Δ_{s} by exploiting only a single image system. Additional information on the cluster mass distribution is needed to break the degeneracy between $\tilde{\kappa}$ and Δ_{s}. This information is, for example, given by dynamical analyses from optical observations of the velocity dispersion of the cluster galaxies (e.g. Wojtak et al. 2007), or from X-ray observations which reveal the luminosity, temperature and location of the intracluster medium (e.g. Vikhlinin et al. 2006).

The information from additional image systems can break this degeneracy, too. By means of a second source plane at redshift z_2, gravitational lensing infers $\kappa(z_2)$. Combining inferences from two source planes at the redshifts z_1 and z_2, one obtains

$$\frac{\kappa(z_1)}{\kappa(z_2)} = \frac{\Delta_1(\Omega)}{\Delta_2(\Omega)} =: \Xi(z_1, z_2, \Omega), \tag{8}$$

where the dependency on the cosmological parameters Ω is explicitly given. This ratio does not depend on the lens mass distribution $\tilde{\kappa}$. By comparing image positions of lensed sources at different redshifts, we can then construct a cosmological probe based on the ratio of distance ratios $\Xi(z_1, z_2, \Omega)$. Fig. 1 shows the isodensity

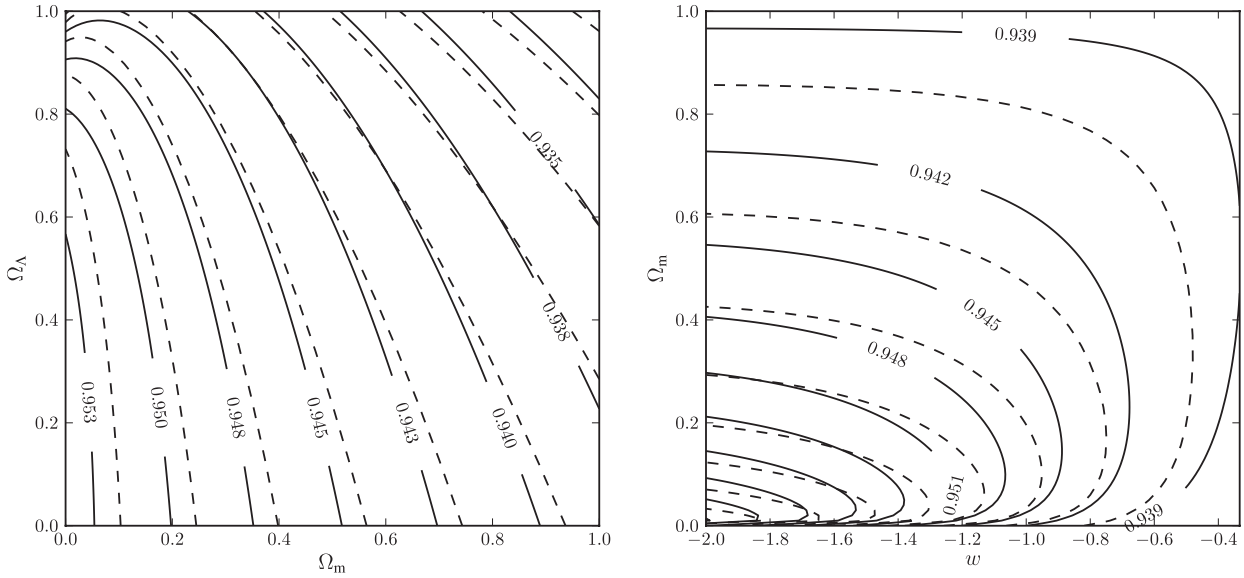

Figure 1. Isodensity contours for $\Xi(z_1, z_2, \Omega)$ with source redshifts $(z_1, z_2) = (1.5, 2.5)$ (solid lines) and $(z_1, z_2) = (2.0, 3.0)$ (dashed lines) are shown in the plane Ω_m–Ω_Λ with $w = -1$ (left-hand panel) and in the plane w–Ω_m with $\Omega_k = 0$ (right-hand panel). The redshift of the lens is $z_l = 0.2$. In the Ω_m–Ω_Λ plane, the contours nearly go in the direction of constant curvature, $\Omega_k = 1 - \Omega_m - \Omega_\Lambda =$ constant. This implies that gravitational lensing is particularly sensitive to the curvature of the universe. Along the isodensity contours, the cosmological information is completely degenerate, but one can break this degeneracy by adding probes with different source redshifts.

contours of $\Xi(z_1, z_2, \Omega)$ for different redshift values in the Ω_m–Ω_Λ plane, as well as in the w–Ω_m plane, where a flat universe is assumed. The cosmological information is completely degenerate along the contours, where the value for Ξ is constant. We can break this degeneracy by combining data from three or more source planes.

In the left-hand panel, the degeneracy nearly goes in the direction of constant curvature, meaning that gravitational lensing is particularly sensitive to the curvature of the universe.

2.2 Hidden priors

The laws governing gravitational lensing are invariant under specific transformations of some observables, whose physical features by contrast are not (Gorenstein, Shapiro & Falco 1988; Saha 2000). This leads to parameter degeneracies when interpreting observations and inferring physical parameters. In gravitational lensing, all observables except for the time delay are dimensionless, and the inference of κ is invariant under the renormalization by an arbitrary constant μ of the angles $\boldsymbol{\theta}$ and $\boldsymbol{\beta}$. This implies that the inference of the Δ_s does not depend on the radial position of the images, but only on their relative geometrical distribution.

Another relevant degeneracy is the so called mass-sheet (or steepness) degeneracy (Schneider & Sluse 2013), where the corresponding transformation with an arbitrary constant μ is

$$\boldsymbol{\beta} \longrightarrow \mu\boldsymbol{\beta}; \quad (1-\kappa) \longrightarrow \mu(1-\kappa). \tag{9}$$

Although the image structure remains the same, the inferred mass profile changes, since this transformation rescales κ by μ and adds or subtracts the constant mass sheet $(1 - \mu)$ from the lens. This implies that the steepness of the mass profile is degenerate with the unknown source position when exploiting a single redshift image system.

There are many ways in which one can break the mass-sheet degeneracy (Saha 2000). In our case, as there is little chance to measure the time delays of the images or the source absolute magnitude, we can break the degeneracy by again exploiting a second image system. Sources at different redshifts imply different lens equations (1). These equations are then no more simultaneously invariant under the transformation in equation (9), implying that the profile steepness is constrained by $\Xi(z_1, z_2, \Omega)$ in equation (8).

Under the variation of Ω, the values for the distance ratios Δ_s change, and consequently also the inferred steepness. In other words, when the cosmological parameters are set free, the mass-sheet degeneracy cannot be completely broken by exploiting multiple source redshifts. A degeneracy between the profile steepness and the cosmological parameters Ω still remains.

The typical approach when modelling gravitational lenses is to assume parametric models, which require a functional form for the mass profile that is in general not invariant under the transformation in equation (9). This assumption breaks the mass-sheet degeneracy even if the cosmological parameters are set free and therefore leads to unwanted priors when inferring the cosmological parameters, which may have a significant influence on the estimate of the cosmological parameters or at least on their uncertainties.

The inner density slope may vary from cluster to cluster and the best theoretical prediction for it is still debated (Limousin et al. 2013; Newman et al. 2013). Thus, in order to make use of parametric models in the context of cosmological parameter determination, a proper analysis should be devoted to the mass-sheet degeneracy. Considerable effort has been made to break this degeneracy when modelling and reconstructing the mass distribution of galaxies and galaxy clusters from gravitational lensing observations (e.g. Suyu et al. 2012; Collett et al. 2013; Greene et al. 2013; Umetsu 2013). Making use of a non-parametric cluster mass description, Bradač et al. (2004, 2005) combined weak and strong lensing to reconstruct the cluster mass profile and break the mass-sheet degeneracy. In the analysis of time-delay galaxies, Suyu et al. (2010, 2013) broke degeneracies by complementing lensing data with additional information that constrains the lens mass profile, such as the measurements of the stellar velocity dispersion or the mass distribution along the line of sight.

To avoid a biased inference, a detailed analysis of the lens, exploiting observations other than strong gravitational lensing, is required in parametric models. We take an alternative approach and consider the more flexible free-form modelling of gravitational lenses to determine the cosmological parameters exploiting strong-lensing observations alone.

3 FREE-FORM LENS MODELLING

For a general mass distribution, the inversion problem of the lens equation (1) cannot be solved analytically but needs to be treated numerically. Moreover, in free-form reconstruction of gravitational lenses one has to deal with a much higher number of parameters than in parametric models. Crucially, however, the relationship between $\boldsymbol{\alpha}$ and κ in equation (2) is linear due to the weak field limit of gravitational lensing (Schneider et al. 1992). We can therefore discretize the mass distribution into grid cells, or pixels, with constant convergence κ_i and rewrite equation (1) for the jth image at redshift z_j as

$$\Delta_j \tilde{\boldsymbol{\beta}}_j = \boldsymbol{\theta}_j - \Delta_j \sum_i \tilde{\kappa}_i \tilde{\boldsymbol{\alpha}}_i(\boldsymbol{\theta}_j), \tag{10}$$

where $\Delta_j \tilde{\kappa}_i \tilde{\boldsymbol{\alpha}}_i(\boldsymbol{\theta}_j)$ is the contribution to $\boldsymbol{\alpha}$ of the ith pixel, $\tilde{\boldsymbol{\beta}}_j = \boldsymbol{\beta}_j(\Delta_j)^{-1}$, and for all images of the same source the $\tilde{\boldsymbol{\beta}}_j$ and Δ_j are equal. This approach has been followed by Saha & Williams (2004) and Coe et al. (2008). Relations in the form of equation (10) for p observed images construct a system of $2p$ linear equations

$$\mathbf{A}x = b, \tag{11}$$

where $\mathbf{A} \in \mathbb{R}^{2p \times n}$, $b \in \mathbb{R}^{2p}$, is a constant vector composed of $\boldsymbol{\theta}_j(\Delta_j)^{-1}$, and $x \in \mathbb{R}^n$ is a vector composed of n free parameters $\tilde{\kappa}_i$ and $\tilde{\boldsymbol{\beta}}_j$. This system is underdetermined as in general $2p \ll n$. Thus, the solution space of equation (11) is unbounded and we need additional constraints to obtain a non-empty compact solution set. Moreover, some of these solutions are unphysical and have to be excluded.

Together with the constraints on the image positions, we require that the mass profile is well-behaved, i.e. non-negative and smooth (Coles 2008). These simple priors limit the solution space to a finite and physical set. To still maintain the linearity, we impose physically motivated constraints on the problem in the form of a system of m linear inequalities

$$\mathbf{C}x \leq d, \tag{12}$$

where $\mathbf{C} \in \mathbb{R}^{m \times n}$, and $d \in \mathbb{R}^m$ is a constant vector.

We take linear constraints, which impose that (i) the mass must be positive everywhere, (ii) its variations must be smooth, and (iii) the local density gradient must point within 45° of the centre. In addition, (iv) the arrival time order as well as the parity of the images are considered. The conditions (i) and (iv) are trivial requirements to ensure a positive mass density, where the produced images are located at the correct stationary points of the arrival time surface. The astrophysically motivated conditions (ii) and (iii) are required to exclude solutions, which mathematically satisfy the equations but are manifestly unphysical. The smoothness of the profile is achieved by imposing that the density of a pixel be no more than twice the average density of its neighbours (Coles 2008), whereas the condition on the local density gradient guarantees an overall decaying mass density profile.

These criteria are weak and cannot drive the derivation of the mass profile, which is determined by the constraints on the image positions. They only ensure the solutions space to be bounded by requiring the mass density to satisfy some basic physical requirements. Moreover, they have been tested against either synthetic lenses from N-body and hydro simulations (Saha et al. 2006; Saha & Read 2009) or toy models following the NFW, power-law or isothermal profile (Lubini & Coles 2012; Sereno & Zitrin 2012). It is consistently found that as long as the number of multiple images is large enough, the mass profile is determined by the data alone, whereas the priors have only a role in the sampling strategy. An exhaustive discussion and a proper mathematical description of the assumed priors can be found in Coles (2008).

It is important to notice that we deliberately excluded any prior constraints on the steepness of the mass profile. Excluding such constraints is crucial to avoid uncontrolled priors on the cosmological parameters, because the steepness of the mass profile degenerates with cosmological parameters (see Section 5).

The solution set of equation (12) is then a subset of $\mathbb{R}^n$, which is bounded by the m hyperplanes representing the constraints. On the other hand, the solution set of equation (11) is an affine space of $\mathbb{R}^n$ having dimension $n_{\mathrm{dof}} = n - 2p$. Hence, the solution set of our problem is given by the intersection between these two sets, which constructs a non-empty convex polytope S, or simplex, embedded in the affine space. Equation (11) therefore serves to reduce the dimension of the problem from n to n_{dof}.

We are interested in finding the volume of the simplex S. As this is in general not possible, we will derive the volume from an uncorrelated random sample X drawn uniformly from S (see Section 4). These parameter spaces, however, are typically embedded in 100 or more dimensions, and therefore the sampling becomes numerically challenging. To obtain an uncorrelated sample X of points in S, we use the gravitational lens modelling framework GLASS (Lubini & Coles 2012; Coles et al., in preparation), which is designed for free-form lens modelling. GLASS uses a Markov chain Monte Carlo method based on the Metropolis–Hasting algorithm (Metropolis et al. 1953; Hastings 1970) with a symmetric proposal density function, which uses equation (12) to hint at the shape of S. This allows efficient sampling of the parameter space S despite the high dimensionality. The algorithm gives an uncorrelated random sample X, whose distribution is as good as a uniform random sample of S (Lubini & Coles 2012).

4 METHOD

4.1 Occam's razor

The method we propose to infer the probability distribution of the cosmological parameters in strong gravitational lensing observations employs a Bayesian approach for model comparison. A standard method to estimate the cosmological parameters Ω is to append them to the vector of the free parameters x and fit all the parameters together by maximizing the likelihood function. In order to be able to find a best fit, however, more data points than parameters are needed. This is possible in the case of parametric models, as in general the number of image position coordinates is larger than the number of free model parameters. The problem is therefore overdetermined and cannot be solved exactly, but the maximum of the likelihood function can be found. At a first level of inference, assuming flat priors, the probability distribution of the parameters Ω is then given by the likelihood function marginalized over the other model parameters x.

In our case, the number of parameters is much larger than the data points. Hence, the number of solutions is infinite, i.e. all $x \in S$ exactly solve equation (1) and have the same likelihood with $\chi^2 = 0$. We are therefore not able to determine the best-fitting parameters using Bayesian first level inference. At the second level of inference, we can estimate the plausibility of different models, given the data, even in an underdetermined case. This is possible because of Bayesian Occam's razor for model comparison (Mackay 2003), where the plausibility of a model is proportional to the volume occupied by S in the parameter space.

The Occam factor for the cosmological parameters in free-form lens modelling is derived as follows. Let us consider different gravitational lens mass reconstruction models $\mathcal{M}_l$ which reproduce the data $\mathcal{D}$ given by the image positions, each time assuming different values of Ω_l for the cosmological parameters. The model $\mathcal{M}_l$ is then described by the cosmological parameters and the setting parameters defining the discretized convergence map. The free parameters x of these models are the mass of the pixels and the source position coordinates, whereas the posterior probability of our problem is given by Bayes' theorem as

$$P(x|\mathcal{D}, \mathcal{M}_l) = \frac{P(\mathcal{D}|x, \mathcal{M}_l) P(x|\mathcal{M}_l)}{P(\mathcal{D}|\mathcal{M}_l)}. \tag{13}$$

Assuming flat priors for the models, which means that $P(\mathcal{M}_l)$ is constant, the probability of a model, given the data, is proportional to the evidence $P(\mathcal{D}|\mathcal{M}_l)$ in equation (13). Marginalizing over x we obtain

$$P(\mathcal{M}_l|\mathcal{D}) \propto P(\mathcal{D}|\mathcal{M}_l) = \int_{\mathbb{R}^n} P(\mathcal{D}|x, \mathcal{M}_l) P(x|\mathcal{M}_l)\, \mathrm{d}x. \tag{14}$$

On the one hand, the prior $P(x|\mathcal{M}_l)$ can be obtained considering equations (11) and (12), and assuming that the data $\mathcal{D}$, i.e. the positions of the images, are unknown (see Section 4.2). These equations define the region $R_l \subset \mathbb{R}^n$, in which x is allowed a priori by the model $\mathcal{M}_l$ before the data arrive. Since only for $x \in R_l$ these equations are exactly satisfied, the prior $P(x|\mathcal{M}_l)$ is uniform in R_l and vanishes outside. That means for $x \in R_l$

$$P(x|\mathcal{M}_l) = 1/V(R_l), \tag{15}$$

where $V(R_l)$ is the volume of R_l. On the other hand, since only for $x \in S_l \subset R_l$ the data $\mathcal{D}$ are exactly reproduced by the model $\mathcal{M}_l$, the likelihood reads

$$P(\mathcal{D}|x, \mathcal{M}_l) = \begin{cases} 1 & \text{if } x \in S_l \\ 0 & \text{if } x \notin S_l \end{cases}. \tag{16}$$

From equations (15) and (16) the evidence in equation (14) can be reduced to

$$P(\mathcal{D}|\mathcal{M}_l) = \int_{S_l} P(x|\mathcal{M}_l)\, \mathrm{d}x = \frac{V(S_l)}{V(R_l)}. \tag{17}$$

This ratio is called the Occam factor and it is the ratio between the posterior and the prior accessible volumes in the parameter space (Mackay 2003). As the purpose of this paper is to obtain confidence levels for the cosmological parameters, we are only interested in the Bayes factor

$$\frac{P(\mathcal{M}_1|\mathcal{D})}{P(\mathcal{M}_2|\mathcal{D})} = \frac{V(S_1)\, V(R_2)}{V(S_2)\, V(R_1)}, \tag{18}$$

where the probabilities of the models assuming either Ω_1 or Ω_2 are compared. Assumptions causing a small collapse of the space volume after the data arrive, i.e. high Occam factor, are favoured compared to the one having a larger collapse (Mackay 2003). Thus, we estimate the plausibility of the parameters Ω by means of equation (18), where the volumes of S and R have to be computed.

4.2 Probability computation

Computing the volumes of such simplices, however, is not without its own problems, since it has been shown that computing the exact volume of a convex polytope is #P-hard, even if all its vertices are known (Dyer & Frieze 1988). We are therefore not able to compute $V(S)$ in high dimensions, because the number of vertices has a huge combinatorial upper bound (McMullen & Shephard 1971). An approximation of $V(S)$ is therefore needed. As we are only interested in ratios between volumes in equation (18), the volume of a simplex can be well approximated by means of its covariance matrix Σ through

$$V(S) \simeq \sqrt{\det \Sigma} = \prod_{i=1}^{n_{\mathrm{dof}}} \sqrt{\lambda_i}, \tag{19}$$

where λ_i are the eigenvalues of Σ. This means that we approximate the true volume $V(S)$ with the volume of an n_{dof}-dimensional ellipsoid or hyperrectangle, whose axis lengths correspond to the square root of the eigenvalues of Σ.

To estimate Σ we use the covariance matrix $\widehat{\Sigma}$ of a sample of points X uniformly and randomly distributed in S, which, as detailed in Section 3, we achieve using the program GLASS. Since the simplex S, and therefore also X, is embedded in an n_{dof}-dimensional affine space, the matrix $\widehat{\Sigma} \in \mathbb{R}^{n \times n}$ is singular, and all the $n - n_{\mathrm{dof}} = 2p$ eigenvalues of $\widehat{\Sigma}$, whose eigenvectors are perpendicular to the affine space, vanish. The sample size $|X|$ has, accordingly, to be $\geq n_{\mathrm{dof}} + 1$, and the points of X must not lie on the same $(n_{\mathrm{dof}} - 1)$-dimensional hyperplane of $\mathbb{R}^n$, meaning that n_{dof} eigenvalues of $\widehat{\Sigma}$ have to be strictly positive. Moreover, to reasonably estimate Σ, samples with $|X| \gg n_{\mathrm{dof}}$ are needed. When too few points are used, especially in high dimensions, the product in equation (19) will have a huge statistical uncertainty due to the randomness of the sampling.

As already stated above, the prior accessible volume $V(R)$ is given considering equations (11) and (12), and assuming $\mathcal{D}$ to be unknown. $V(R)$ simply reflects the degeneracy in equation (7), i.e. the fact that the smaller the distance ratios Δ_s, the larger the value of the convergence $\tilde{\kappa}$, and, finally, the larger $V(R)$. On the one hand, in equation (12) the constraints on the arrival time and the parity are unknown, whereas the remaining constraints, which consist of the smoothness constraints of the mass distribution, the constraints on the local gradient, and $\kappa_i \geq 0$, can all be written in the form $c \cdot x \leq 0$, where c is a constant vector. Therefore, the solution set is bounded by hyperplanes passing through the origin of the parameter space. Hence, these constraints do not depend on the norm $\|x\|$, which implies that the model-dependent part of equation (12) constrains only the solid angle of R. This is shown schematically as the grey region in Fig. 2. It is important to notice that only the information obtained from lensing observations and not the additional constraints of equation (12) constrains the norm $\|x\|$ and thus the mass of the pixels.

On the other hand, as the unknown data imply unknown $\boldsymbol{\theta}$ and $\mathbf{A}$, the solution set of equation (11) is an affine space with an unknown angular position. The solid angle as well as the angular position of R does not depend on Ω and is therefore equal for all $\mathcal{M}$. The only cosmological parameter dependent part in these equations is given by the vector b in equation (11), since its components are proportional to $\Delta_j(\Omega)^{-1}$. The distance d between the affine space and the origin of the parameter space is defined by

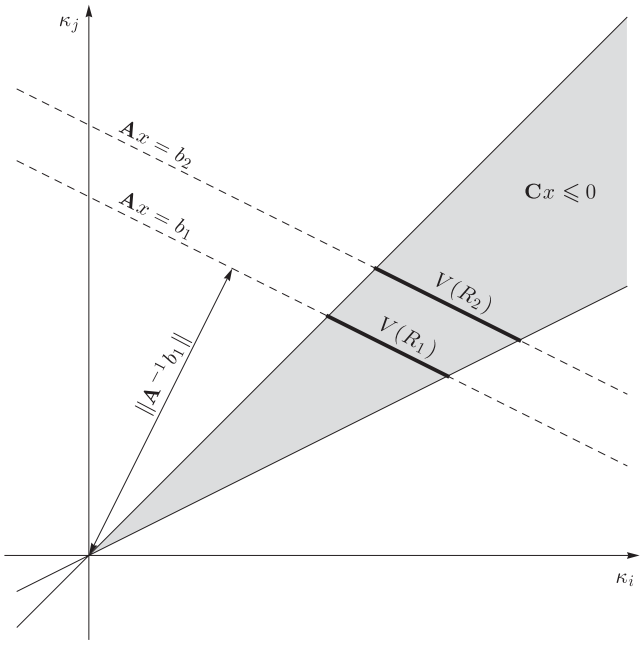

Figure 2. The prior accessible volume $V(R)$ is shown schematically for two different cosmological parameter assumptions Ω_1 and Ω_2. Here a two-dimensional graph is shown for simplicity, where $x = (\kappa_i, \kappa_j)$. The equation $\mathbf{C}x \leq 0$ constrains the solid angle of R, whereas the equation $\mathbf{A}x = b$ defines the affine solution space. The only Ω-dependent part in these two equations is the vector b. The volumes $V(R_1)$ and $V(R_2)$ are then proportional to $d_1 = \|\mathbf{A}^{-1}\, b_1\|$ and $d_2 = \|\mathbf{A}^{-1}\, b_2\|$, since in this case $n_{\rm dof} = 1$.

b through

$$d = \|\mathbf{A}^{-1}\, b\|, \tag{20}$$

where $\mathbf{A}^{-1}$ denotes the Moore–Penrose pseudo-inverse of $\mathbf{A}$. Since $\boldsymbol{\theta}$ and $\mathbf{A}$ are unknown, we assume random values for their components, implying that

$$d \,\widetilde{\propto}\, \langle \Delta_j(\Omega)^{-1} \rangle, \tag{21}$$

where $\langle \cdot \rangle$ is the arithmetic mean over the images j. For the probability ratio in equation (18), it is enough to consider the cosmological parameter dependent part, which for the volume of R is given by

$$V(R) \propto d^{n_{\rm dof}} \propto \mathcal{H}(\Delta_j(\Omega_l))^{-n_{\rm dof}}, \tag{22}$$

where $\mathcal{H}(\cdot)$ is the harmonic mean over the images j. Fig. 2 shows schematically the volumes $V(R_1)$ and $V(R_2)$ obtained considering two different affine spaces, where the vectors b_1 and b_2 correspond to Ω_1 or Ω_2, respectively. The volumes are then proportional to $d_1^{n_{\rm dof}}$ and $d_2^{n_{\rm dof}}$, respectively. In this example, $n_{\rm dof} = 1$, since for simplicity we show a two-dimensional plot.

Considering equations (19) and (22), we obtain the final estimate for the probability of a cosmological model $\mathcal{M}_l$, given the data $\mathcal{D}$, which reduces to

$$P(\mathcal{M}_l|\mathcal{D}) \propto \left(\prod_{i=1}^{n_{\rm dof}} \sqrt{\widehat{\lambda}_{l,i}} \right) \cdot \mathcal{H}(\Delta_j(\Omega_l))^{n_{\rm dof}}, \tag{23}$$

where $\widehat{\lambda}_{l,i}$ are the $n_{\rm dof}$ positive eigenvalues of $\widehat{\Sigma}_l$. To better understand this result, let us consider the special case of a single source redshift $z_{\rm s}$. The harmonic mean then reduces to $\mathcal{H}(\Delta_j(\Omega_l)) = \Delta_{\rm s}(\Omega_l)$ and equation (10) can be rewritten in the variables $\kappa_i = \tilde{\kappa}_i \cdot \Delta_{\rm s}(\Omega_l)$ and $\boldsymbol{\beta}_j = \tilde{\boldsymbol{\beta}}_j \cdot \Delta_{\rm s}(\Omega_l)$ for all the images j. Thus, the factor $\Delta_{\rm s}(\Omega_l)$ cancels out in equation (10), which does not depend anymore on the choice of Ω_l. The simplex S_l in the $(\tilde{\kappa}_i, \tilde{\boldsymbol{\beta}}_j)$ space can be transformed into the corresponding simplex S' in the $(\kappa_i, \boldsymbol{\beta}_j)$ space simply by multiplying the coordinates with the factor $\Delta_{\rm s}(\Omega_l)$. Hence, for equation (23) we obtain

$$P(\mathcal{M}_l|\mathcal{D}) \propto V(S_l) \cdot \Delta_{\rm s}(\Omega_l)^{n_{\rm dof}} = V(S'), \tag{24}$$

meaning that the probability is proportional to the volume of the simplex in the $(\kappa_i, \boldsymbol{\beta}_j)$ space. By construction, $V(S')$ does not depend on the choice of Ω_l, and thus neither does $P(\mathcal{M}_l|\mathcal{D})$. As expected from the discussion in Section 2, regarding the degeneracy in equation (7), we cannot constrain cosmological parameters with a single source plane.

In the case of multiple source redshifts, since κ_i depends on the redshift of the source, there are many different $(\kappa_i, \boldsymbol{\beta}_j)$ spaces. Hence, instead of $V(S')$ in equation (23) we have to consider an average of the volumes of the simplices in the $(\kappa_i, \boldsymbol{\beta}_j)$ spaces to be proportional to the probability. For this reason, the factor $\mathcal{H}(\Delta_j(\Omega_l))^{n_{\rm dof}}$ is required in equation (23), and thus it accounts for the degeneracy in equation (7).

5 TESTS

We test our method by means of synthetic lenses produced with GRAVLENS (Keeton 2001a,b). This software builds lenses as parametric mass distributions and finds, through numerical inversion of the lens equation (1), the position, the arrival time and the parity of all the images produced by a given source position. Image configurations $\mathcal{D}$ are produced by the synthetic lenses assuming a reference set of true cosmological parameters $\Omega_{\rm ref}$. This is a realistic testing procedure, since our method utilizes a discretized mass distribution, whereas the adopted image configurations are obtained from smooth lenses, just as real galaxies or galaxy clusters. For simplicity and without loss of generality, we renormalize each image position $\boldsymbol{\theta}$ by the mean radius $\langle \|\boldsymbol{\theta}_j\| \rangle$ of all the images. This leaves the results unchanged (see Section 2) and allows for an easier comparison between different configurations and mass profiles.

For each cosmological model, by means of GLASS, we then find a set X of discretized mass distributions and source positions, i.e. $x \in S_l$, which exactly reproduce the synthetic image configuration.

The discretized mass distribution is defined within a radius R, which is divided into P pixels (Saha & Williams 2004). Thus, the models $\mathcal{M}_l$ depend not only on Ω_l but also on the model parameters R and P. While the latter changes the resolution of the discretization, R does not influence n. We fix P a priori and marginalize over R, that is,

$$P(\Omega_l, \mathcal{M}|\mathcal{D}) = \int_{\mathbb{R}} P(\Omega_l, R, \mathcal{M}|\mathcal{D})\, {\rm d}R, \tag{25}$$

where the dependency on Ω_l and R is written explicitly. The marginalization with respect to R is important, since for different Ω_l the probabilities may have their maximum at different R. Moreover, this procedure enables us to exclude those image configurations where $P(\Omega_l, R, \mathcal{M}|\mathcal{D})$ as a function of R is not single peaked or heavily depends on the choice of Ω_l. Without accounting for different map radii, cosmological information would be strongly affected by the discretization and thus no longer reliable.

To test the model, we consider a realistic scenario, where the lens located at redshift $z_{\rm l} = 0.2$ is a massive cluster, which follows a single NFW profile with concentration parameter $c_{200} = 5$, mass $M_{200} = 10^{15}\, {\rm M}_\odot\, h^{-1}$ and ellipticity $e = 0.15$. To produce the synthetic image configurations in this section, we assume a ΛCDM

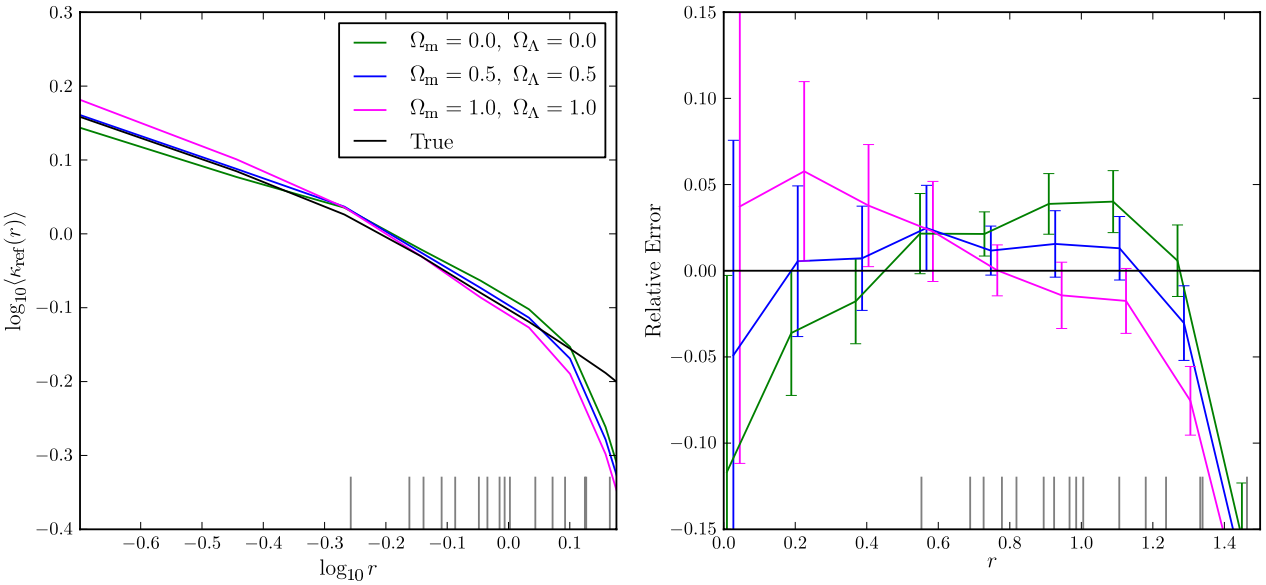

Figure 3. Left-hand panel: The reconstructed lens profile κ_{ref} ($z_{ref} = 2$) of the same lens is shown for three different sets of cosmological parameters. Only the assumed values for $\Omega = (\Omega_m, \Omega_\Lambda)$ change between the reconstructions. $\langle\kappa_{ref}(r)\rangle$ is the mean of κ_{ref} within the pixelated ring of radius r, which is in units of $\langle\|\boldsymbol{\theta}_j\|\rangle$. The images, whose positions are marked by grey lines, are located at radii $0.55 \le r \le 1.46$, or $-0.26 \le \log_{10} r \le 0.16$. For comparison, the true mass profile, used to produce the image systems under the assumption of $\Omega_{ref} = (0.5, 0.5)$, is shown in black. The fits are not physical outside the outermost images, since there is no lensing information on the mass profile. Right-hand panel: To highlight the degeneracy between steepness and cosmological parameters, the relative error with respect to the true mass profile $\kappa_{ref}/\kappa_{true} - 1$ is shown. The three curves in the plot have been slightly shifted to avoid the overlapping of the 1σ error bars.

cosmological model with $\Omega_{ref} = (\Omega_m, \Omega_\Lambda) = (0.5, 0.5)$. Results for this reference cosmological model are then compared to two competitive models, the empty open universe $\Omega_{emp} = (0, 0)$ and a closed universe, $\Omega_{cld} = (1, 1)$.

As discussed in Section 2, the mass-sheet degeneracy is still there even after exploiting multiple source redshifts and setting Ω free. We consider an image configuration with five different source planes producing overall 16 images, whose redshifts are $z_s = 1.0, 1.5, 2.0, 2.5$ and 3.0, respectively. The mean mass profiles for the three fits are shown in Fig. 3. The profile steepness depends on the assumed cosmological parameters. Cosmologies with a larger Ω_k need a shallower mass profile in order to fit the given configuration. The fit with the correct value for Ω excellently reproduces the true mass profile within the outermost image radius. Thus, GLASS is able to reproduce the assumed profile and produces an unbiased mass estimate (Lubini & Coles 2012).

Outside the outermost image position there is no information on the profile and the fits are unphysical. This is because in equation (12) we consider moderate constraints and let the steepness of the profile completely free to vary in order to avoid breaking any possible degeneracy as, for instance, the mass-sheet degeneracy. This issue, however, has no influence on our analysis, as these pixels are not constrained by the images and thus are independent of Ω_l. Nevertheless, these pixels have to be considered, since otherwise the approximation $V(S) \simeq (\det \widehat{\Sigma})^{1/2}$ in equation (19) is no longer valid.

We elucidate and test some properties of equation (23) by means of an image configuration with three sources producing overall $p = 12$ images, i.e. three quads, whose source redshifts are $z_s = 1.0, 2.0$ and 3.0, respectively. We produce solution sets X with $|X| = 10^4$ and $P = 8$, which implies that there are $n = 231$ free parameters. The sorted list of the eigenvalues $\widehat{\lambda}_i$ in the case with $R = 1.85$ is shown in the left-hand panel of Fig. 4. Only the first $n_{dof} = 207$ eigenvalues are strictly positive, whereas the remaining $2p = 24$ eigenvalues vanish, as expected. The larger eigenvalues correspond to the more massive pixels, i.e. those located in the very inner region of the mass distribution. The mass-sheet degeneracy is therefore also visible in the steepness of the curves of the three different cosmologies.

The right-hand panel of Fig. 4 shows $P(\Omega_l, R, \mathcal{M}|\mathcal{D})$ as a function of R for the three sets of cosmological parameters. The curves are single peaked with the maximum around $R = 1.85$ and the curve corresponding to the true cosmological parameters has a larger normalization than the others. The marginalization over R yields the probabilities $P(\Omega_l, \mathcal{M}|\mathcal{D})$. The true cosmology is clearly favoured with $P(\Omega_{ref}, \mathcal{M}|\mathcal{D})$ being about three times larger than $P(\Omega_{emp}, \mathcal{M}|\mathcal{D})$ and $P(\Omega_{cld}, \mathcal{M}|\mathcal{D})$.

We finally verified that the method is unbiased to the underlying cosmological model of reference. Even assuming the extreme case $\Omega_{ref} = (\Omega_m, \Omega_\Lambda) = (2.5, 0.5)$ our method could find Ω_{ref} within the uncertainties.

6 PARAMETER DETERMINATION

To show the accuracy of the method, we considered the massive cluster with $(c_{200}, M_{200}, e) = (5, 10^{15}\,\mathrm{M}_\odot\,h^{-1}, 0.15)$ of Section 5 and the concordance ΛCDM cosmology with $\Omega_{ref} = (\Omega_m, \Omega_{de}, w) = (0.27, 0.73, -1)$ (Komatsu et al. 2011) as the 'true' cosmological model. The synthetic image configuration is produced by five sources at redshifts $z_s = 1.2, 1.9, 2.5, 2.8$ and 4.0, which produce three quads and two doubles. The total of 16 images at different redshifts contain the information on the cosmography.

We fit the parameters either in the Ω_m–Ω_Λ plane, where $(\Omega_m, \Omega_\Lambda) \in [0, 1] \times [0, 1]$ with $w = -1$, or in the w–Ω_m plane, where $(w, \Omega_m) \in [-2, -1/3] \times [0, 1]$ and $\Omega_k = 0$. We divided the two planes into grids, and computed the probabilities $P(\Omega_l, \mathcal{M}|\mathcal{D})$ marginalizing over R for each model Ω_l.

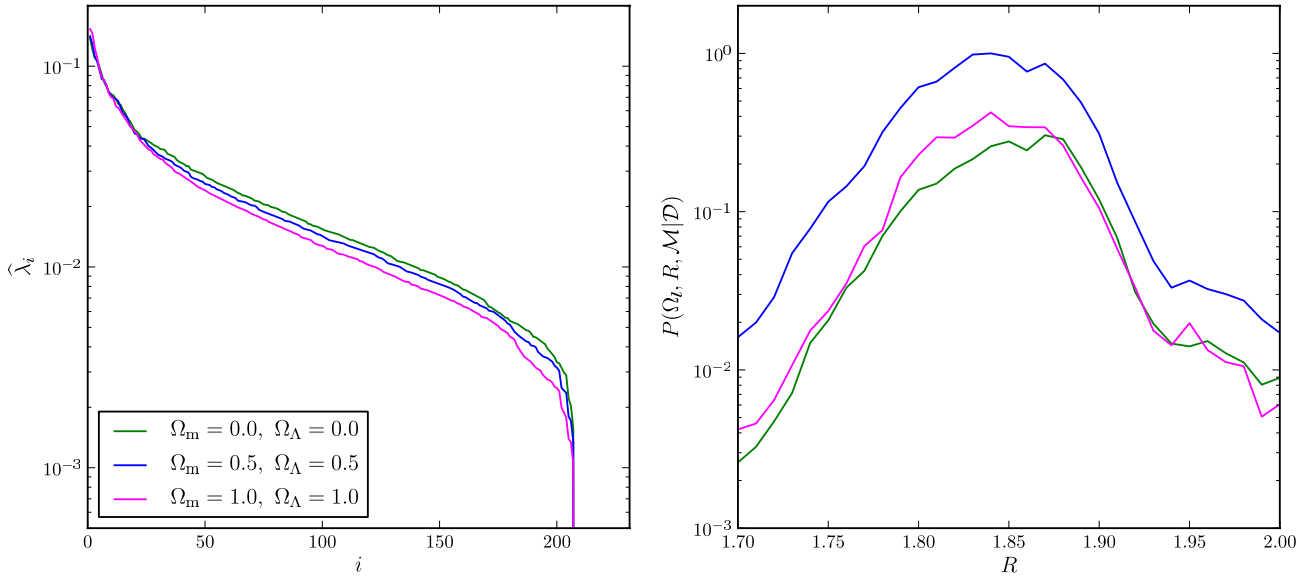

Figure 4. Left-hand panel: The sorted list of the eigenvalues $\widehat{\lambda}_i$ of $\widehat{\Sigma}$ for the three different fits with $|X| = 10^4$ and $R = 1.85$ is shown. The first $n_\mathrm{dof} = 207$ eigenvalues are strictly positive, whereas the last $n - n_\mathrm{dof} = 2p = 24$ eigenvalues are not displayed, as they are $<10^{-14}$, which means 0 within the machine precision. Right-hand panel: The probability $P(\Omega_l, R, \mathcal{M}|\mathcal{D})$ as a function of R is shown for the three fits. The three curves were rescaled in arbitrary units. The blue curve corresponding to Ω_ref is larger than the other two cases, meaning that this assumption is more likely.

Although the sampling algorithm has been recently improved, it still has a running time of $\mathcal{O}(n^3)$ (Lubini & Coles 2012). Thus, we need to keep the space dimension small enough to have a reasonable computation time, but large enough such that the discretization does not compromise the fit of the image configuration. For this reason, we choose $P = 8$, which corresponds to $n = 235$, and divide the planes into grids of 21×21 and 21×17 pixels, respectively.

The results are shown for the Ω_m–Ω_Λ plane in the left-hand panel of Fig. 5, and for the w–Ω_m plane in the right-hand panel. The probability isodensity contours follow those in Fig. 1, since for gravitational lensing the information of the cosmological parameters is contained in Ξ. The parameter degeneracy is partially broken, thanks to the multiple source redshifts.

The method is mainly sensitive to the space curvature parameter Ω_k and the matter density parameter Ω_m in the Ω_m–Ω_Λ plane, and to the dark energy equation of state w in the w–Ω_m plane. These parameters are almost perpendicular to the degeneracies in the respective planes, and can therefore be inferred by means of a single lens even if with large uncertainties.

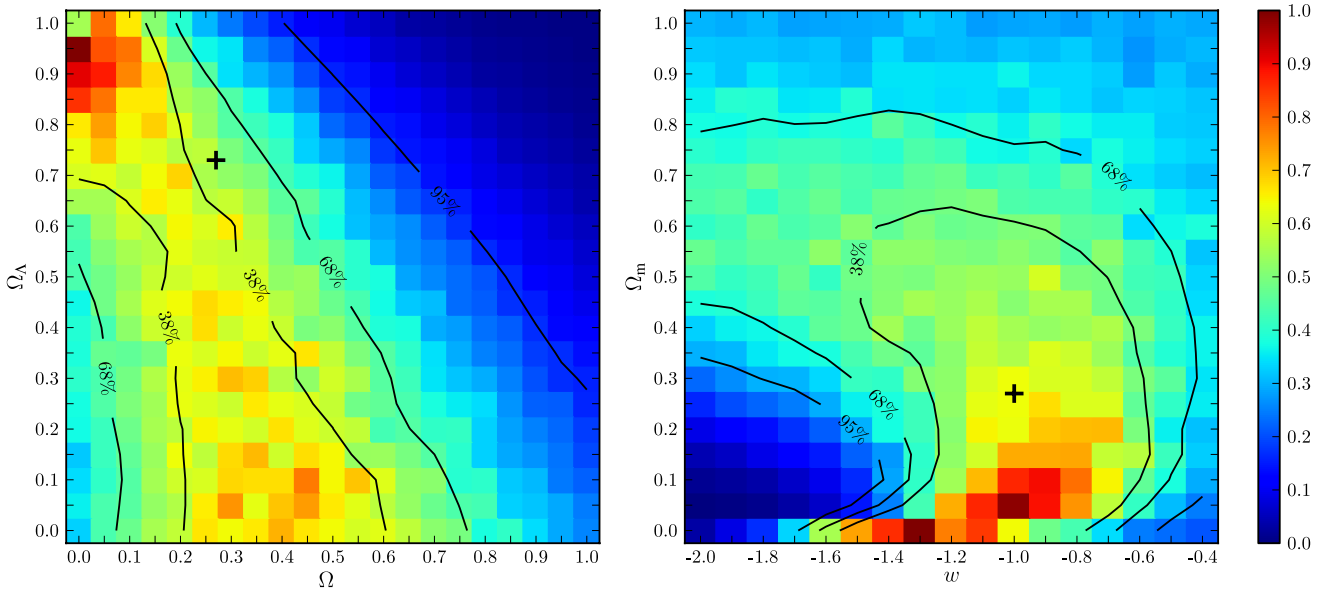

Figure 5. The inferred probability distribution for a single lensing cluster in the Ω_m–Ω_Λ plane with $w = -1$ (left-hand panel) and in the w–Ω_m plane with $\Omega_k = 0$ (right-hand panel). The probability isodensity contours almost correspond to the contours shown in Fig. 1 and the area enclosed by the contours corresponds to, respectively, 38, 68 and 95 per cent of the total probability. The true values for the cosmological parameters $\Omega_\mathrm{ref} = (0.27, 0.73, -1)$ are shows by the black crosses.

Our method obtains an unbiased estimate of the assumed values for the cosmological parameters within the statistical uncertainties. Ω_k is retrieved with an accuracy of 0.3 and w with an uncertainty of about 0.4, whereas Ω_m is accurate within 0.3.

7 CONCLUSIONS

Strong gravitational lensing exploiting multiple lensed background sources in galaxy clusters is a unique tool to probe the cosmology. It relies on purely geometrical information that does not need any calibration, and explores new redshift ranges around $z \sim 3$–4. To extract the cosmological information contained in lensed image systems, we exploited free-form lens modelling by means of the framework GLASS. This software is based on an efficient sampling strategy that produces uncorrelated random samples (Lubini & Coles 2012). These are fundamental for our analysis, since the solution spaces we need to sample are convex polytopes in 200 and more dimensions.

The free-form approach we investigated is more flexible than parametric techniques, and requires only the geometrical information from strong lensing. Parametric models demand deep knowledge of all cluster components, and assume functional forms for the mass profiles, which break the mass-sheet degeneracy. When inferring the cosmological parameters, however, the mass-sheet degeneracy is still present even in the case of multiple source planes, since cosmologies with larger Ω_k need shallower mass profiles to fit the same image configuration. Therefore, parametric models unintentionally break possible degeneracies by adding hidden priors to the analysis. This leads to biased estimates with unrealistically small uncertainties.

Our method does not use constraints on the steepness of the profile and accounts for the mass-sheet degeneracy. This solves one of the main systematics in lensing determination of cosmological parameters. The systematic effect due to the presence of uncorrelated substructures along the line of sight (D'Aloisio & Natarajan 2011), which is a main source of uncertainty in cosmography, has not been considered in this paper. However, cosmic variance plays a minor role in the strong-lensing regime.

Since in free-form modelling there are more free parameters than data points, we cannot follow a maximum-likelihood estimation of the cosmological parameter. Therefore, we developed a method based on Bayesian model comparison. The probabilities are obtained through the Occam factor, which means that we take the volume of the solution space as a tracer of the probability. We considered the probability to be proportional to the ratio between the posterior and prior accessible volumes.

Testing with synthetic lenses showed that our method can infer the values of the assumed cosmological parameters. The free-form strong-lensing geometrical test we developed seems particularly promising in view of ongoing and future observational programmes. The Cluster Lensing And Supernova survey with Hubble (CLASH) project (Postman et al. 2012) has been deeply observing 25 massive clusters at $0.2 \lesssim z \lesssim 0.6$. Predictions and first analyses (Umetsu et al. 2012; Zitrin et al. 2012; Medezinski et al. 2013) agree on an expected detection rate of at least between 12 and 15 multiple systems per cluster. On the basis of the CLASH clusters alone, the strong-lensing test we proposed might decrease the uncertainties of the cosmological parameters with respect to ones obtained for one single cluster in Section 6 by almost one order of magnitude.

Future surveys will provide additional very large cluster samples. *Euclid* is expected to detect about 5000 clusters with prominent arcs and strong-lensing features (Laureijs et al. 2011). The consequent improvement of the method accuracy over such a large sample is of one or two additional orders of magnitude. The performance should further improve using the method in combination with orthogonal probes such as CMB or BAOs.

REFERENCES

Abdelsalam H. M., Saha P., Williams L. L. R., 1998a, MNRAS, 294, 734
Abdelsalam H. M., Saha P., Williams L. L. R., 1998b, AJ, 116, 1541
Amanullah R., Lidman C., Rubin D., Aldering G., Astier P., Barbary K., Burns M. S., Conley A., 2010, ApJ, 716, 712
Bolton A. S., Burles S., Koopmans L. V. E., Treu T., Gavazzi R., Moustakas L. A., Wayth R., Schlegel D. J., 2008, ApJ, 682, 964
Bradač M., Lombardi M., Schneider P., 2004, A&A, 424, 13
Bradač M., Schneider P., Lombardi M., Erben T., 2005, A&A, 437, 39
Coe D., Fuselier E., Benítez N., Broadhurst T., Frye B., Ford H., 2008, ApJ, 681, 814
Coles J., 2008, ApJ, 679, 17
Collett T. E. et al., 2013, MNRAS, 432, 679
D'Aloisio A., Natarajan P., 2011, MNRAS, 411, 1628
Deb S., Goldberg D. M., Ramdass V. J., 2008, ApJ, 687, 39
Diego J. M., Sandvik H. B., Protopapas P., Tegmark M., Benítez N., Broadhurst T., 2005, MNRAS, 362, 1247
Dyer M. E., Frieze A. M., 1988, SIAM J. Comput., 17, 967
Falco E. E., Gorenstein M. V., Shapiro I. I., 1985, ApJ, 289, L1
Gilmore J., Natarajan P., 2009, MNRAS, 396, 354
Golse G., Kneib J.-P., Soucail G., 2002, A&A, 387, 788
Gorenstein M. V., Shapiro I. I., Falco E. E., 1988, ApJ, 327, 693
Greene Z. S. et al., ApJ, 768, 39
Hastings W. K., 1970, Biometrika, 57, 97
Jullo E., Natarajan P., Kneib J.-P., D'Aloisio A., Limousin M., Richard J., Schimd C., 2010, Science, 329, 924
Keeton C. R., 2001a, preprint (astro-ph/0102340)
Keeton C. R., 2001b, preprint (astro-ph/0102341)
Komatsu E., Smith K. M., Dunkley J., Bennett C. L., Gold B., Hinshaw G., Jarosik N., Larson D., 2011, ApJS, 192, 18
Laureijs R. et al., 2011, preprint (arXiv:1110.3193)
Liesenborgs J., de Rijcke S., Dejonghe H., Bekaert P., 2007, MNRAS, 380, 1729
Limousin M. et al., 2007, ApJ, 668, 643
Limousin M., Morandi A., Sereno M., Meneghetti M., Ettori S., Bartelmann M., Verdugo T., 2013, Space Sci. Rev., 177, 155
Lubini M., Coles J., 2012, MNRAS, 425, 3077
Mackay D. J. C., 2003, Information Theory, Inference and Learning Algorithms. Cambridge Univ. Press, Cambridge
McMullen P., Shephard G. C., 1971, Convex Polytopes and the Upper Bound Conjecture. Cambridge Univ. Press, Cambridge
Medezinski E. et al., 2013, ApJ, 777, 43
Metropolis N., Rosenbluth A. W., Rosenbluth M. N., Teller A. H., Teller E., 1953, J. Chem. Phys., 21, 1087
Navarro J. F., Frenk C. S., White S. D. M., 1996, ApJ, 462, 563
Navarro J. F., Frenk C. S., White S. D. M., 1997, ApJ, 490, 493
Newman A. B., Treu T., Ellis R. S., Sand D. J., Nipoti C., Richard J., Jullo E., 2013, ApJ, 765, 24
Percival W. J., Reid B. A., Eisenstein D. J., Bahcall N. A., Budavari T., Frieman J. A., Fukugita M., Gunn J. E., 2010, MNRAS, 401, 2148
Planck Collaboration et al., 2013, preprint (arXiv:1303.5076)
Postman M. et al., 2012, ApJS, 199, 25
Read J. I., Saha P., Macciò A. V., 2007, ApJ, 667, 645
Richard J., Pei L., Limousin M., Jullo E., Kneib J. P., 2009, A&A, 498, 37
Riess A. G. et al., 2011, ApJ, 730, 119
Saha P., 2000, AJ, 120, 1654
Saha P., Read J. I., 2009, ApJ, 690, 154
Saha P., Williams L. L. R., 2004, AJ, 127, 2604
Saha P., Coles J., Macciò A. V., Williams L. L. R., 2006, ApJ, 650, L17
Schneider P., Sluse D., 2013, A&A, 559, A37

Schneider P., Ehlers J., Falco E. E., 1992, Gravitational Lenses. Springer-Verlag, Berlin
Schneider P., Kochanek C., Wambsganss J., 2006, Gravitational Lensing: Strong, Weak and Micro. Springer-Verlag, Berlin
Sereno M., 2002, A&A, 393, 757
Sereno M., Longo G., 2004, MNRAS, 354, 1255
Sereno M., Zitrin A., 2012, MNRAS, 419, 3280
Sereno M., Lubini M., Jetzer P., 2010, A&A, 518, A55
Sereno M., Ettori S., Umetsu K., Baldi A., 2013, MNRAS, 428, 2241
Soucail G., Kneib J.-P., Golse G., 2004, A&A, 417, L33
Suyu S. H., Marshall P. J., Auger M. W., Hilbert S., Blandford R. D., Koopmans L. V. E., Fassnacht C. D., Treu T., 2010, ApJ, 711, 201
Suyu S. H. et al., 2012, ApJ, 750, 10
Suyu S. H. et al., 2013, ApJ, 766, 70
Umetsu K., 2013, ApJ, 769, 13
Umetsu K. et al., 2012, ApJ, 755, 56
Vikhlinin A., Kravtsov A., Forman W., Jones C., Markevitch M., Murray S. S., Van Speybroeck L., 2006, ApJ, 640, 691
Voit G. M., 2005, Rev. Mod. Phys., 77, 207
Weinberg S., 1972, Gravitation and Cosmology: Principles and Applications of the General Theory of Relativity. Wiley, New York
Wojtak R., Łokas E. L., Mamon G. A., Gottlöber S., Prada F., Moles M., 2007, A&A, 466, 437
Zieser B., Bartelmann M., 2012, preprint (arXiv:1204.0372)
Zitrin A. et al., 2012, ApJ, 749, 97

This paper has been typeset from a TEX/LATEX file prepared by the author.